Reflection-contrast limit of fiber-optic image guides

Pierre M. Lane
Calum E. MacAulay
British Columbia Cancer Agency
675 West 10th Avenue
Vancouver, British Columbia V5Z 1L3
Canada

Abstract. Fiber-optic image guides in confocal reflectance endomicroscopes introduce background backscatter that limits the achievable contrast in these devices. We show the dominant source of backscatter from the image guide is due to Rayleigh scattering at short wavelengths and terminal reflections of the fibers at long wavelengths. The effective Rayleigh scattering coefficient and the wavelength-independent reflectivity due terminal reflections are measured experimentally in a commercial image guide. The Rayleigh scattering component of backscatter can be accurately predicted using the fractional refractive-index difference and length of the fibers in the image guide. We also presented a simple model that can be used to predict signal-to-background ratio in a fiber-optic confocal reflectance endomicroscope for biologically relevant tissues and contrast agents that cover a wide range of reflectivity.
[DOI: 10.1117/1.3269679]

Keywords: confocal; image guide; fiber optic; microendoscopy; endomicroscopy; Rayleigh scatter; reflectance; contrast.

Paper 09345R received Aug. 7, 2009; revised manuscript received Sep. 29, 2009; accepted for publication Oct. 6, 2009; published online Dec. 7, 2009.

1 Introduction

Confocal endomicroscopes use one or more optical fibers to simultaneously deliver illumination light and return reflected or fluorescent light to a detector.[1–3] Distally scanned devices employ a single optical fiber[4] (or a pair of illumination-detection fibers[5]) and miniature scanner distal to the fiber, while proximally scanned devices[1,6,7] use a fiber-optic image guide to simplify probe design. The image guide of a proximally scanned device introduces background backscatter to the detected signal that, when used in reflectance mode, can be difficult to discriminate from the backscatter of interest generated by the tissue. Endomicroscopes used in fluorescence mode do not have this problem because the image-guide backscatter is attenuated by the same filters that block reflected excitation light from the sample.

Studies involving confocal reflectance microscopy of surgical specimens[8–11] have shown that reflectance contrast has great potential for disease diagnosis and, importantly, does not require the application of contrast agents. Fibered image-guide systems for confocal fluorescence endomicroscopy have been deployed for pilot clinical trials by several research groups,[12,13] and a commercial system is available from Mauna Kea Technologies (Paris). Even though reflection contrast can provide diagnostic imagery, there have been few devices reported in the literature[7] and no systems are available commercially. The reason for this is likely the technical challenges involved in achieving sufficient reflection contrast due to image-guide backscatter.

In this paper, we determine the limit of contrast for the class of confocal reflectance endomicroscopes that employ a fiber-optic image guide. A model of terminal reflections in a fiber-optic image guide and a method to minimize them was presented in a previous paper.[14] We showed that it was difficult to completely attenuate image-guide backscatter. In this paper, we show that image-guide backscatter is due to terminal backreflections from the two ends of the image guide and Rayleigh scatter from within the fibers. We derive an expression to describe Rayleigh scatter in a fiber-optic image guide, measure the Rayleigh scattering coefficient of a commercial image guide, and propose a model to predict signal-to-backscatter ratio for a biologically relevant tissues and contrast agents that cover a wide range of reflectivities.

2 Theory

The problem of Rayleigh backscatter in a single-mode optical fiber was first treated by Brinkmeyer[15] as a deterministic process. The author derived an expression for Rayleigh backscatter due to an optical pulse assuming a completely incoherent source. Gysel and Staubli[16] derived an equivalent expression for mean backscatter for the case of a continuous wave (coherent) input source. The latter is more appropriate for application to an image guide and is given by

$$\frac{\langle I_b \rangle}{I_0} = \alpha_R S \frac{1 - \exp(-2\alpha L)}{2\alpha}, \quad (1)$$

where $\langle I_b \rangle$ is the mean backscattered intensity, I_0 is the source intensity, α_R is the Rayleigh scattering attenuation constant, α is the total power attenuation constant, S is the backscatter recapture factor, and L is the fiber length. The total attenuation includes both absorption and scattering losses but not losses due to mode coupling between multiple fibers. The

Address all correspondence to: Pierre M. Lane, British Columbia Cancer Agency, 675 West 10th Avenue, Vancouver, British Columbia V5Z 1L3, Canada. Tel: 604-675-8087; Fax: 604-675-8099; E-mail: plane@bccrc.ca

1083-3668/2009/14(6)/064028/7/$25.00 © 2009 SPIE

mean backscattered intensity is independent of source coherence (i.e., bandwidth), and its power spectral density is twice that of the source.[16]

The Rayleigh scattering attenuation constant is given by[17]

$$\alpha_R = \frac{1}{\lambda^4}\frac{\int A(r)P(r)rdr}{\int P(r)rdr} = \frac{\bar{A}}{\lambda^4}, \quad (2)$$

where λ is the wavelength, $A(r)$ is the local Rayleigh scattering coefficient, $P(r)$ is the local light intensity in the fiber, and r is the radial coordinate of the fiber. The distribution of power and Rayleigh scattering coefficient depends on the refractive index profile of the fiber and its normalized frequency. It is convenient to describe the Rayleigh scattering coefficient as an effective or average value $\bar{A}$ as defined in Eq. (2).

The transmission of an individual fiber is determined by fiber attenuation and additional losses due to cross talk (mode coupling) with other fibers in the bundle. For short image guides typical of confocal endomicroscopy, attenuation due to cross talk is the dominant factor and fiber attenuation can be ignored. In the limit as total attenuation goes to zero, the last term in Eq. (1) can be simplified as follows:

$$\lim_{\alpha\to 0}\frac{1-\exp(-2\alpha L)}{2\alpha} = L. \quad (3)$$

We now add a term to account for the dominant attenuation mechanism in a fiber-optic image guide, cross-coupling. The oscillatory cross-coupling of power in an image guide takes place over centimeters to tens of centimeters.[18] We therefore consider the average power propagating in the fiber to be reduced by a factor, $\bar{T}_c$ the average transmission of an individual fiber due to cross-coupling. The exact fraction of power lost due to cross-coupling is periodic in length and wavelength and quite difficult to predict because it depends on the size and shape of the fibers involved. We therefore use an empirically determined average transmission to account for the cross-coupling between fibers.

An expression for Rayleigh backscatter in a fiber-optic image guide may then be derived by combining Eqs. (1)–(3) and incorporating $\bar{T}_c$ as discussed to obtain

$$\frac{\langle I_b\rangle}{I_0} = \frac{\bar{A}LS\bar{T}_c}{\lambda^4}. \quad (4)$$

The refractive index profile of an optical fiber is created by doping pure silica glass with specific impurities. Unfortunately, this doping also leads to increased Rayleigh scatter. The refractive index of silica glass increases with GeO_2 doping concentration and decreases with F doping concentration. Ohashi et al. measured Rayleigh scattering and refractive index difference in fiber performs[17] and proposed the following empirical formula to predict Rayleigh scattering:

$$\bar{A} = A = \begin{cases} A_0[1+41\Delta] & \text{F-doped silica} \\ A_0[1+44\Delta] & GeO_2\text{-doped silica} \end{cases}, \quad (5)$$

where $\Delta = (n_1^2 - n_2^2)/2n_1^2$ is the fractional refractive index difference, n_1 and n_2 are the refractive indices of the GeO_2-doped core and silica cladding (or silica core and F-doped cladding), respectively, and $A_0 = 0.8$ (in decibels per quadrupled micrometers per kilometers) is the Rayleigh scattering coefficient of pure silica. We have made the assumption in Eq. (5) that the effective Rayleigh scattering coefficient is equal to the Rayleigh scatter coefficient at the peak index difference. This simplifies calculations when the exact index profile and power distribution are not known, and it is equivalent to assuming that power is confined to the core of the fiber.

The backscatter recapture factor (or fraction of backscattered light captured and transmitted in the opposite direction) depends on the refractive index profile of the fiber (step or graded index) and number of propagating modes (single or multimode). The backscatter recapture factor for a graded (parabolic) index fiber operating below cutoff (multimode) is given by[19]

$$S = \frac{1}{4}\frac{n_1^2 - n_2^2}{n_1^2} = \left(\frac{NA}{2n_1}\right)^2 = \frac{\Delta}{2}, \quad (6)$$

where NA is numerical aperture, and for step-index fibers the factor of 1/4 is replaced by 3/8. In single-mode fibers, the backscatter recapture factor satisfies $0.21(n_1^2 - n_2^2)n_1^{-2} \leq S \leq 0.24(n_1^2 - n_2^2)n_1^{-2}$.[15]

This section has highlighted some useful relationships that can be used to drive the development of new devices. Equation (4) illustrates that Rayleigh scatter is proportional to image guide length, and as expected, inversely proportional to wavelength to the fourth power. This suggests devices with short image guides operating in the long-wavelength region will achieve the highest signal to background levels. Rayleigh scatter is proportional to doping concentration in the core as predicted by Eqs. (4) and (5). Therefore, image guides with low doping concentrations in the core (ideally pure silica with F-doped cladding) are preferred over images guides with Ge-doped cores. Rayleigh backscatter is also directly proportional to the fractional refractive index difference of the image guide through the recapture factor and consequently Rayleigh backscatter increases quadratically with fiber NA.

3 Materials, Methods, and Analysis

3.1 *Measurement of Rayleigh Scatter*

3.1.1 *Experimental setup*

A schematic diagram of the experimental setup used to measure Rayleigh scatter as a function of wavelength is shown in Fig. 1. Light from a Ti:sapphire laser (Coherent Chameleon) was coupled into one arm of a broadband −3-dB fiber coupler (Thor Labs, p/n FC850-40-50-APC). Light from one of the output fibers was optically relayed onto the proximal end of the fiber-optic image guide under test. The optical replay consisted of a fiber port (Thor Labs, p/n PAF-X-7-B) and an aspheric lens (LightPath Technologies, p/n 350340). A microscope slide placed between the image guide and the asphere allowed a refractive index coupling oil to be placed between

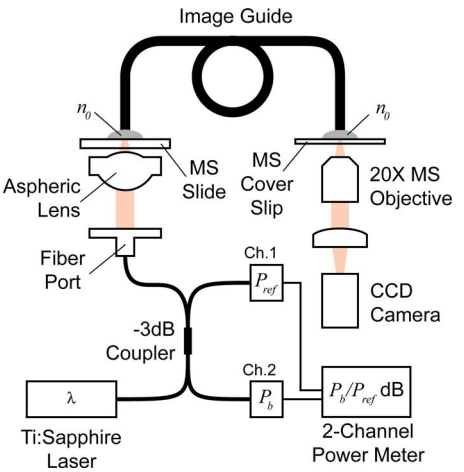

Fig. 1 Schematic illustration of the experimental setup used to measure Rayleigh scatter as a function of wavelength. Backscatter is measured using a two-channel power meter. Focus and alignment of the image guide with the illumination spot is performed while observing the image on the CCD camera.

the slide and the image guide. A coupling oil (Cargille Labs, Cedar Grove, New Jersey) with refractive index $n=1.4920$ was used to match the average index of the fiber cores.[14] All refractive indices are specified at 589.3 nm and 25 °C. The aspheric lens was on a z-axis stage to focus the spot on the proximal face of the image guide, and the image guide was held in an x-y stage to allow different fibers in the image guide to be illuminated.

A microscope coverslip was optically coupled to the distal end of the image guide using the same coupling oil as the proximal end to minimize backreflections. A 20X microscope objective and CCD camera were employed at the distal end to facilitate coupling the spot at the proximal end of the image guide into a single fiber and to quantify the light intensity coupled into the fibers of the image guide. Coupling the illumination spot into a single fiber required that the spot first be focused while monitoring the image of the distal end of the image guide on the CCD camera and then the spot could be translated to illuminate different fibers in the image guide.

The remaining two ports of the fiber coupler were coupled to a two-channel power meter (Newport 2931 -C with 918D-UV photodetectors). Channel 2 measured the backreflected power from the image guide P_b, and channel 1 measured a power reference P_{ref}. The power meter was set to report the referenced power ratio P_b/P_{ref} in decibels. The Ti:sapphire laser was tuned to 750, 800, 850, 900, and 950 nm, and the Rayleigh backscatter from the image guide was measured at each wavelength in triplicate. The image guide was refocused at each wavelength to correct for the axial chromatic aberration of the aspheric lens. The backscatter measurements were normalized to the power incident on the image guide to correct for the spectral transmission of the optical components. The proximal end of the image guide was replaced with the channel 1 detector to measure the referenced incident power P_0/P_{ref} on the image guide at each wavelength. The referenced incident power was subtracted from the corresponding referenced backscattered power to give the backscattered power relative to incident power, P_b/P_0. An image of the distal end of the image guide was also acquired at each wavelength so that that the average power transmitted by the target fiber could be quantified.

We measured Rayleigh backscatter from a Sumitomo image guide (p/n IGN-08/30). This image guide has 30,000 graded-index fibers on 3-μm centers, an NA of 0.35, and an outside diameter of 1 mm. The image guide was 3 m long and was measured as-shipped from Sumitomo without cutting or repolishing the ends. The vendor specified an average core refractive index of 1.49 (1.50 on axis) and a cladding refractive index of 1.45.[20]

3.1.2 *Rayleigh scatter model*

The backscattered data were fit to a simple linear model,

$$\frac{P_b}{P_0} = \frac{c}{\lambda^4} + \mathcal{R}_0, \tag{7}$$

which is functionally equivalent to the expression for Rayleigh backscatter derived previously in Eq. (4). The model is linear in reciprocal wavelength to the fourth power and has two parameters: constant $\mathcal{R}_0$ is wavelength-independent backscatter and slope

$$c = \bar{A}LS\bar{T}_c, \tag{8}$$

encapsulates the four parameters introduced in Eq. (4). The length of the fiber was known, the backscatter recapture factor was calculated using Eq. (6), and the refractive indices were provided by the vendor. We calculated the effective Rayleigh scattering coefficient for each fiber.

The average transmission of the measurement fiber due to cross-coupling was determined from the CCD images acquired from the distal face of the image guide. The image pixels corresponding to fiber cores were segmented, and the power propagating in each fiber was calculated as the sum of all pixel intensities belonging to that fiber. The transmission of the measurement fiber was calculated as the power of the measurement fiber divided by the sum of all fiber powers. The average transmission $\bar{T}_c$ was calculated as the sum of the transmissions at each wavelength divided by the number of wavelengths.

3.2 *Prediction of Background Backscatter*

Background backscatter of a fiber-optic image guide was predicted from the fractional refractive index difference and compared to the experimentally measured data points. We used Eqs. (7) and (8) to model backscatter, Eq. (5) to predict the Rayleigh scatter coefficient from the fractional refractive index difference of the image guide and the Rayleigh scatter coefficient of pure silica, and Eq. (6) to calculate the backscatter recapture factor. Image guide parameters $(L, \bar{T}_c, n_1, n_2)$ were chosen to be identical to those of the experimental image guide to allow for direct comparison, and we used the experimentally measured value for the constant (terminal) reflection $\mathcal{R}_0$.

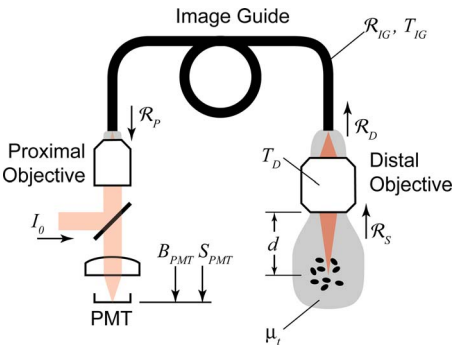

Fig. 2 Schematic diagram illustrating the image-guide contrast model for a reflection-mode confocal endomicroscope. The model is used to compute the signal-to-background ratio at different wavelengths.

3.3 *Signal-to-Background Ratio (SBR) Model*

A schematic diagram illustrating the image-guide contrast model for a reflection-mode confocal endomicroscope is show in Fig. 2. The aim is to model SBR

$$\frac{S_{\mathrm{PMT}}}{B_{\mathrm{PMT}}} = \frac{T_{\mathrm{D}}^2(1-\mathcal{R}_{\mathrm{D}})^2 T_{\mathrm{IG}}^2(1-\mathcal{R}_{\mathrm{P}})^2}{\mathcal{R}_{\mathrm{D}}(1-\mathcal{R}_{\mathrm{P}})^2 T_{\mathrm{IG}}^2 + (1-\mathcal{R}_{\mathrm{P}})^2\mathcal{R}_{\mathrm{IG}} + \mathcal{R}_{\mathrm{P}}}\mathcal{R}_{\mathrm{S}}, \quad (9)$$

where signal S_{PMT} is defined to be backscatter from the focal volume under investigation and background B_{PMT} is defined to be unwanted backscatter due to Rayleigh scatter and terminal reflections from the image guide. Signal contrast generated by the biological sample has reflectivity $\mathcal{R}_{\mathrm{S}}$ at the input to the distal objective. T_{D} and T_{IG} are the transmissions of the distal objective and image guide, $\mathcal{R}_{\mathrm{P}}$ and $\mathcal{R}_{\mathrm{D}}$ are the reflections at the proximal and distal ends of the image guide, and $\mathcal{R}_{\mathrm{IG}}$ is the Rayleigh backscatter from the image guide itself.

SBR was plotted using Eq. (9) and the experimentally determined values for image-guide Rayleigh scatter and terminal reflections (the mean value for the constant reflection $\mathcal{R}_0$ was divided equally between the two terminal reflections). We modeled four biologically relevant tissues and/or contrast agents, specifically, amelanotic tissue, amelanotic with acetic acid, melanotic tissue, and gold nanoparticles, to span the entire range of reflectivity. Reflectivity at the input to the distal objective was approximated for each tissue and/or contrast agent using

$$\mathcal{R}_{\mathrm{S}} = \exp(-2d\mu_t)\left(\frac{n_1-n_2}{n_1+n_2}\right)^2 = \exp(-2d\mu_t)\left(\frac{\Delta n}{2\bar{n}}\right)^2, \quad (10)$$

where $\Delta n = n_1 - n_2$ is the refractive index difference that generates the reflectance signal and $\bar{n} = (n_1+n_1)/2$ is the mean refractive index. We used values typical of confocal microscopy for the imaging depth $d = 100$ (in microns) and the total attenuation coefficient $\mu_t = 100$ (per centimeter).[21] Refractive index data found in the literature was used to calculate reflectivity at the focal volume of each tissue or contrast agent. Refractive index data and calculated reflectivities are summarized in Table 1.

Table 1 Refractive index data and calculated target reflectivity.

Contrast Target	Refractive index: Difference	Refractive index: Average	Reflectivity $\mathcal{R}_S$ (dB)
Amelanotic tissue	$\Delta n = 0.05$ [21]	$\bar{n} = 1.40$[a]	−44
Amelanotic tissue with acetic acid	$\Delta n = 0.12$ [27]	$\bar{n} = 1.39$[a]	−36
Melanotic tissue	$n_1 = 1.70$ (melanin)[b]		−28
	$n_2 = 1.37$ (cytoplasm)[c]		
Gold nanoparticle film	$n_1 = 2.56 + i1.11$ (Au)[d]		−17
	$n_2 = 1.37$ (cytoplasm)[c]		

[a]Ref. 27.
[b]Ref. 28.
[c]Ref. 29.
[d]Ref. 30.

4 Results

Measured backscatter data are plotted in Fig. 3. The plot shows reciprocal wavelength on the abscissa and measured backscatter on the ordinate. Data points and error bars indicate backscatter measurements for three fiber cores selected at random from the image guide. The lines show the best fit to the linear model of Eq. (7). Best-fit parameters, standard errors, and 95% confidence intervals are shown in Table 2. The measured fiber transmission due to cross-coupling, calculated backscatter recapture factor, and Rayleigh scatter coefficients calculated from the measured data are shown in Table 3 for each fiber core. Instrumentation backscatter was measured to be −56.2 dB without the aspheric lens installed and −55.9 dB with the aspheric lens and microscope slide installed but without the image guide.

5 Discussion

5.1 *Measurement of Rayleigh Scatter*

The experimental setup employed optical components with very low backreflection so they did not contribute to the measured backscatter signal. The minimum detectable reflectance

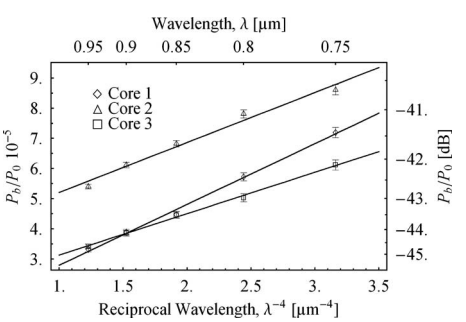

Fig. 3 Backscatter versus reciprocal wavelength for three fiber cores. The fiber cores were selected at random from a commercial image guide (Sumitomo IGN 08/30). Data points and error bars represent measured data while the lines are a linear least-square fit for each data set.

Table 2 Linear least-squares fit results.

IG core	$\hat{c}$ (10^{-6} μm^4)		$\mathcal{R}_0$ (dB)		R^2
	Est±SE	95% CI	Est±SE	95% CI	
1	20.1±0.7	(17.8, 22.4)	−51.0±0.9	(−55.4, −48.9)	0.996
2	16.6±1.3	(12.4, 20.8)	−44.5±0.3	(−45.8, −43.5)	0.981
3	13.7±0.4	(12.4, 15.1)	−47.5±0.2	(−48.3, −46.9)	0.997
Mean	16.8±0.9	(15.0, 18.6)	−46.9±0.4	(−47.8, −46.2)	

was limited by the directivity of the fiber-optic coupler, which was specified by the manufacturer to be >55 dB. The coupler employed FC/APC (FC type, angled physical contact) connectors to reduce terminal reflection below −65 dB. An aspheric lens design to image through a 1.2-mm window was used instead of a multielement microscope objective lens to minimize the backreflections from the lens. We did not subtract instrumentation backscatter from the experimental measurements because the instrumentation backscatter was 10 times lower. In order to minimize terminal reflections from the image guide, the spot projected onto its proximal face had a mode field diameter of 3 μm and NA 0.26 to match the average geometry of the fiber cores. The coupling oil had similar dispersion characteristics to that of fused silica, and consequently, the dependence of the terminal reflections on wavelength was negligible.

The model of Eq. (7) was appropriate as indicated by the high values for goodness of fit ($R^2 > 0.98$) in Table 2. The backscatter signal is quite different between cores as illustrated by the significant variation in slope and offset between the three data sets plotted in Fig. 3. The slopes of the best-fit lines describe the intensity of the Rayleigh scatter while the offsets (y intercepts) describe the wavelength-independent component due to the terminal reflections. The variation in Rayleigh intensity (slope) is most likely due to differences in fiber transmission due to cross-coupling rather than differences in Rayleigh scatter coefficient, backscatter recapture factor, or fiber length [see Eq. (8)]. This is supported by numerical analysis,[18] which shows that the coupling between fiber modes of an image guide is very sensitive to variation in core size and shape. The variation in constant backscatter between the three data sets is probably due to slight differences in termination between the three fiber cores. We have shown that it is not possible to exactly index match all fiber cores simultaneously due to the variation in size and shape of the fibers.[14] Rayleigh scatter and terminal reflections therefore should be measured and corrected on a per fiber basis rather than on a global basis to be most effective; however, this is not practical in an image guide with many fibers.

5.2 *Prediction of Image-Guide Backscatter*

Predicted and measured background backscatter from the fiber-optic image guide is plotted in Fig. 4, which illustrates the two sources of inherent backscatter—Rayleigh scatter and terminal reflections. Background backscatter is dominated by Rayleigh scatter at short wavelengths and by terminal reflections at long wavelengths.

The image-guide backscatter predicted using the fractional refracitve index difference of the image guide matches well with the experimental measurements from Fig. 3. The Rayleigh scatter component of the backscatter is calculated entirely from basic image-guide parameters (core and cladding refractive indices, length, and transmission) while the experimental measured value is used for the terminal reflection component. The Rayleigh scatter coefficient calculated from the fiber's refractive index difference was less than the measured values reported in Table 3; however, the calculated value was still within the standard error of the mean measurement. The doping concentration in the core and cladding (and refractive index profile) would be better predictors of the Rayleigh scatter coefficient;[22] however, these data are generally proprietary and not published by image-guide vendors. The Rayleigh scattering coefficient of GeO_2 and F co-doped glass is reported[23] to be linear in GeO_2 concentration and quadratic in F concentration. Other factors, such as fiber-drawing tem-

Table 3 Transmission due cross coupling and calculated Rayleigh scatter coefficients.

IG core	Recapture factor S	Length L (m)	Transmission $\bar{T}_c$	Model parameter $\bar{c}$ (10^{-6} μm^4)	RS coefficient A (dB μm^4 km^{-1})
1	0.016	3	0.95±0.05	20.1±0.7	2.9±0.9
2			0.94±0.04	16.6±1.3	2.4±0.8
3			0.72±0.24	13.7±0.4	2.6±1.5
Mean			0.87±0.14	16.8±0.9	2.6±1.1

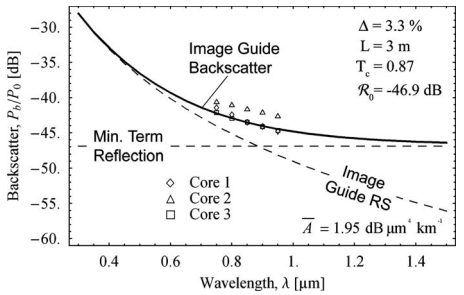

Fig. 4 Background backscatter from a fiber-optic image guide. The figure illustrates the two sources of inherent backscatter—Rayleigh scatter and terminal reflections. Background backscatter (solid curve) is dominated by Rayleigh scatter (dashed curve) at short wavelengths and by terminal reflections (dashed horizontal line) at long wavelengths. The measured data from Fig. 3 are also shown.

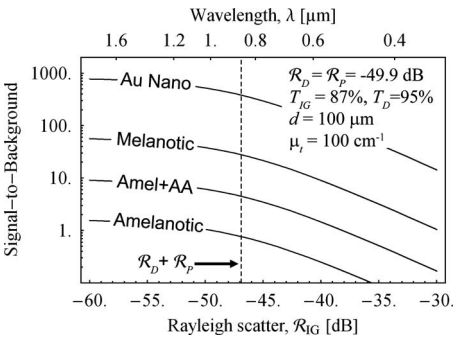

Fig. 5 Predicted SBR versus image-guide Rayleigh scatter. SBR is shown for the cases of amelanotic tissue, amelanotic tissue contrast-enhanced with acidic acid, melanotic tissue, and gold nanoparticles. The minimum terminal reflection (dashed vertical line) divides the abscissa into terminal-reflection limited (left) and Rayleigh-scatter limited (right) operating regions.

perature, annealing treatment, and drawing speed, have also been shown to influence Rayleigh scattering,[22,24] but these factors were not considered here.

It may be possible to reduce Rayleigh backscatter in an image guide using pure silica fiber cores with F-doped cladding (to reduce the Rayleigh scatter coefficient) and smaller fractional reflective index differences (to reduce recoupling of Rayleigh scatter). Telecom fiber (Corning SMF-28) generates 25 times less Rayleigh backscatter than image-guide fiber due primarily to its smaller reflective index difference.

5.3 *SBR Model*

The SBR model compares the signal detected from four biologically relevant contrast targets that cover a wide range of reflectivities to the magnitude of background scatter due to the image guide. This allows the prediction of SBR for the contrast targets as a function of wavelength (due to Rayleigh scatter) and terminal reflections.

The model of Eq. (9) is derived by following optical power as it is transmitted, reflected, and backscattered through the system. The five squared factors in the numerator correspond to attenuation of the signal in the forward and backward directions due to attenuation in the sample, transmission of the distal objective, the two image-guide terminal reflections, and transmission of the image guide. The three terms in the numerator correspond to the three sources of attenuated backscatter noise, namely, Rayleigh scatter and the two terminal reflections from the image guide. The sources of backscatter noise are assumed to add incoherently.

The reflectance at the entrance to the distal objective due to the biologically relevant targets is approximated using Eq. (10). Refractive index changes between cellular components produce the greatest source of contrast in confocal reflectance images of the microscopic structure of tissue.[21,25] We assume that reflectivity is given simply by power reflectance at normal incidence multiplied by an exponential to account for absorption and scattering.

Contrast in amelanotic tissue is generated by the refractive index differences between organelles (mitochondria lysomes, peroxisomes) and subcomponents of organelles (chromatin material in the nucleus) and there surrounding medium.[21,26,27] The amelanotic reflectivity is calculated from the refractive index difference for amelanotic tissue from Smithpeter et al.,[2] and the mean cellular refractive index from Drezek et al.[27] The topical application of acetic acid to amelanotic tissue increases nuclear scattering due to changes in the refractive index structure of the nucleus. The reflectivity of amelanotic tissue stained with acetic acid was calculated assuming its nuclear refractive index difference doubles after the application of acidic acid while the mean nuclear index remains constant.[27] Contrast in melanotic tissue is provided by the refractive index difference between melanin granules and the surrounding cytoplasm.[8] The reflectivity for melanotic tissue was calculated using the refractive indices for melanin[28] and cytoplasm.[29] The reflectivity of gold nanoparticles was approximated using the refractive index data for a gold nanoparticle film.[30]

The significance of the SBR model is illustrated in Fig. 5. As shown, the gold nanoparticles and melanotic tissue provide sufficient (>1) SBR over the entire range of Rayleigh scatter considered; however, the SBR for amelanotic tissue, both with and without acetic acid as a contrast enhancer, is only practical when image-guide Rayleigh scatter is low. The vertical dashed line indicating the sum of the terminal reflections divides the plot into terminal-reflection-limited and Rayleigh-scatter-limited operating regions (the line indicates total termination backscatter equals Rayleigh backscatter). The best imaging performance is achieved at longer wavelengths where backscatter due to Rayleigh scatter is less than that due to the terminal reflections.

In a previous paper, we showed that it is not possible to completely eliminate the terminal reflections from the image-guide fibers.[14] This is due to the gradient index profile of the fibers and the considerable variation in size and shape between fiber cores. A refractive index coupling medium that minimizes the terminal reflection for one fiber at one wavelength is unlikely to minimize all other fibers at the same wavelength due to differences in mode confinement relative to the graded-index profile. In practice, the index-matching medium should be determined empirically at a particular wavelength to minimize the global terminal reflections from all fibers taken together. In Fig. 5, we used the mean value of the wavelength-independent backscatter measurements for the sum of the terminal reflection, $\mathcal{R}_D+\mathcal{R}_P=\mathcal{R}_0=46.9$ dB, as indicated by the dashed vertical line.

As illustrated in Fig. 5, the best SBR is achieved when operating to the left of the dashed line when backscatter noise is terminal-reflection limited. The wavelength axis of Fig. 5 is mapped to the Rayleigh scatter axis assuming an image guide length of 2 m and the experimentally measured values for Rayleigh scatter coefficient $\bar{A}=2.6$ and fiber mode-coupled transmission $\bar{T}_c=0.87$. Therefore, given that terminal reflections have been minimized, SBR is terminal-reflection limited at wavelengths of >860 nm. In this operation region, the SBR for amelanotic tissue will be slightly greater than 1 and will increase to 10 with the addition of acetic acid. Similarly, the SBR is predicted to be 50 for melanotic tissue and several hundred for gold nanoparticles.

6 Conclusions

The SBR of confocal reflectance imaging using a fiber-optic image guide is limited by backscatter due to the image guide. The dominant source of backscatter noise is due to Rayleigh scatter at short wavelengths and due to the terminal reflections of the image guide at long wavelengths. We measured the effective Rayleigh scattering coefficient of fibers in a commercial image guide and the constant (wavelength independent) reflectivity due their terminal reflections. The effective Rayleigh scattering coefficient and constant reflectivity, averaged over three fibers, were $\bar{A}=2.6$ and $\mathcal{R}_0=-46.9$.

The Rayleigh scatter component of image-guide backscatter can be accurately predicted using the fractional refractive index difference of the fibers. The Rayleigh backscatter intensity increases with the length of the image guide, the doping concentration of the fiber core, and the NA of the fiber. We also presented a simple model that can be used to predict SBR in a fiber-optic confocal reflectance endomicroscope for biologically relevant tissues and contrast agents that cover a wide range of reflectivity.

Acknowledgments

This study was supported, in part, by grants from the National Institutes of Health (Grant No. 5-P01-CA096964-02, No. U01-CA96109, and No. 1R01 CA10383) and the National Cancer Institute of Canada (Grant No. 12067). Thank you to Katherine Simons-Lane for her help in acquiring the spectral reflectance data from the image guides.

References

1. A. F. Gmitro and D. Aziz, "Confocal microscopy through a fiberoptic imaging bundle," *Opt. Lett.* **18**(8), 565–567 (1993).
2. C. MacAulay, P. Lane, and R. Richards-Kortum, "*In vivo* pathology: microendoscopy as a new endoscopic imaging modality," *Gastrointest Endosc Clin. N. Am.* **14**(3), 595–620 (2004).
3. K. Sokolov, K. B. Sung, T. Collier, A. Clark, D. Arifler, A. Lacy, M. Descour, and R. Richards-Kortum, "Endoscopic microscopy," *Dis. Markers* **18**(5–6), 269–291 (2002).
4. D. L. Dickensheets and G. S. Kino, "Micromachined scanning confocal optical microscope," *Opt. Lett.* **21**(10), 764–766 (1996).
5. T. D. Wang, C. H. Contag, M. J. Mandella, N. Y. Chan, and G. S. Kino, "Dual-axes confocal microscopy with post-objective scanning and low-coherence heterodyne detection," *Opt. Lett.* **28**(20), 1915–1917 (2003).
6. P. M. Lane, A. L. P. Dlugan, R. Richards-Kortum, and C. E. MacAulay, "Fiber-optic confocal microscopy using a spatial light modulator," *Opt. Lett.* **25**(24), 1780–1782 (2000).
7. K. B. Sung, C. N. Liang, M. Descour, T. Collier, M. Follen, and R. Richards-Kortum, "Fiber-optic confocal reflectance microscope with miniature objective for *in vivo* imaging of human tissues," *IEEE Trans. Biomed. Eng.* **49**(10), 1168–1172 (2002).
8. M. Rajadhyaksha, M. Grossman, D. Esterowitz, R. H. Webb, and R. R. Anderson, "*In -vivo* confocal scanning laser microscopy of human skin—melanin provides strong contrast," *J. Invest. Dermatol.* **104**(6), 946–952 (1995).
9. T. Collier, A. Lacy, R. Richards-Kortum, A. Malpica, and M. Follen, "Near real-time confocal microscopy of amelanotic tissue: detection of dysplasia in *ex vivo* cervical tissue," *Acad. Radiol.* **9**(5), 504–512 (2002).
10. T. Collier, M. Guillaud, M. Follen, A. Malpica, and R. Richards-Kortum, "Real-time reflectance confocal microscopy: comparison of two-dimensional images and three-dimensional image stacks for detection of cervical precancer," *J. Biomed. Opt.* **12**(2), 024021 (2007).
11. A. L. Clark, A. M. Gillenwater, T. G. Collier, R. Alizadeh-Naderi, A. K. El-Naggar, and R. R. Richards-Kortum, "Confocal microscopy for real-time detection of oral cavity neoplasia," *Clin. Cancer Res.* **9**(13), 4714–4721 (2003).
12. J. A. Udovich, A. R. Rouse, A. Tanbakuchi, M. A. Brewer, R. Sampliner, and A. F. Gmitro, "Confocal microendoscope for use in a clinical setting," *Proc. SPIE* **6432**, 64320H (2007).
13. P. M. Lane, S. Lam, A. McWilliams, J. C. leRiche, M. W. Anderson, and C. E. MacAulay, "Confocal fluorescence microendoscopy of bronchial epithelium," *J. Biomed. Opt.* **14**(2), 024008 (2009).
14. P. Lane, "Terminal reflections in fiber-optic image guides," *Appl. Opt.* **48**(30), 5802–5810 (2009).
15. E. Brinkmeyer, "Backscattering in single-mode fibers," *Electron. Lett.* **16**(9), 329–330 (1980).
16. P. Gysel and R. K. Staubli, "Statistical properties of Rayleigh backscattering in single-mode fibers," *J. Lightwave Technol.* **8**(4), 561–567 (1990).
17. M. Ohashi, K. Shiraki, and K. Tajima, "Optical loss property of silica-based single-mode fibers," *J. Lightwave Technol.* **10**(5), 539–543 (1992).
18. K. L. Reichenbach and C. Xu, "Numerical analysis of light propagation in image fibers or coherent fiber bundles," *Opt. Express* **15**(5), 2151–2165 (2007).
19. E. G. Neumann, "Analysis of the backscattering method for testing optical fiber cables," *AEU, Int. J. Electron. Commun.* **34**(4), 157–160 (1980).
20. N. Kuwamura, Sumitomo Electric USA, Inc. (personal communication) (2009) .
21. C. L. Smithpeter, A. K. Dunn, A. J. Welch, and R. Richards-Kortum, "Penetration depth limits of *in vivo* confocal reflectance imaging," *Appl. Opt.* **37**(13), 2749–2754 (1998).
22. Z. Wang, G. B. Ren, S. Q. Lou, and S. S. Jian, "Loss properties due to Rayleigh scattering in different types of fiber," *Opt. Express* **11**(1), 39–47 (2003).
23. K. Tsujikawa, M. Ohashi, K. Shiraki, and M. Tateda, "Scattering property of F and Geo2 codoped silica glasses," *Electron. Lett.* **30**(4), 351–352 (1994).
24. K. Tsujikawa, K. Tajima, K. Shiraki, and I. Sankawa, "Method for predicting Rayleigh scattering loss of silica-based optical fibers," *J. Lightwave Technol.* **25**(8), 2122–2128 (2007).
25. A. K. Dunn, C. Smithpeter, A. J. Welch, and R. Richards-Kortum, "Sources of contrast in confocal reflectance imaging," *Appl. Opt.* **35**(19), 3441–3446 (1996).
26. C. Smithpeter, A. Duan, R. Drezek, T. Collier, and R. Richards-Kortum, "Near real time confocal microscopy of cultured amelanotic cells: sources of signal, contrast agents and limits of contrast," *J. Biomed. Opt.* **3**(4), 429–436 (1998).
27. R. Drezek, A. Dunn, and R. Richards-Kortum, "Light scattering from cells: finite-difference time-domain simulations and goniometric measurements," *Appl. Opt.* **38**(16), 3651–3661 (1999).
28. I. A. Vitkin, J. Woolsey, B. C. Wilson, and R. R. Anderson, "Optical and thermal characterization of natural (sepia-officinalis) melanin," *Photochem. Photobiol.* **59**(4), 455–462 (1994).
29. A. Brunstin and P. F. Mullaney, "Differential Light-Scattering from Spherical Mammalian-Cells," *Biophys. J.* **14**(6), 439–453 (1974).
30. H. L. Zhang, S. D. Evans, and J. R. Henderson, "Spectroscopic ellipsometric evaluation of gold nanoparticle thin films fabricated using layer-by-layer self-assembly," *Adv. Mater.* **15**(6), 531–534 (2003).